

# Spectra and Decay Properties of Higher Lying $B_c$ Meson States

Nayana T S<sup>1,\*</sup> and Bhaghyesh<sup>1,†</sup>

<sup>1</sup>*Department of Physics, Manipal Institute of Technology,  
Manipal Academy of Higher Education, Manipal 576104, India.*

In this work, the spectra and decay properties of  $B_c$  mesons ( $c\bar{b}$ ) have been investigated using a non-relativistic potential model incorporating corrections from LQCD. The non-relativistic Schrodinger wave equation is solved numerically using the Matrix Numerov Method. Using the obtained masses and wave functions, decay widths, lifetime, branching ratios and radiative decay widths are computed for the  $c\bar{b}$  system. We compare the obtained results with the experimental data and with other theoretical models.

Keywords:  $B_c$  mesons; non-relativistic potential model; LQCD corrections; matrix numerov method; radiative decays

## I. INTRODUCTION

$B_c$  mesons are open flavored mesons consisting of a heavy quark and a heavy antiquark of dissimilar flavors ( $c\bar{b}$  or  $b\bar{c}$ ) with a net non-zero charge. Energy levels of  $B_c$  mesons lies in between that of charmonium ( $c\bar{c}$ ) and bottomonium ( $b\bar{b}$ ). Due to similarity with hidden flavor quarkonia,  $B_c$  mesons provide an opportunity to validate the potentials and formalisms used to study charmonium and bottomonium states [1, 2]. Spectroscopic study of  $B_c$  mesons will provide us important information on heavy quark dynamics and help us extract various parameters of the electroweak theory [1]. Experimentally, only very few  $c\bar{b}$  states have been discovered. It is expected that more states would be discovered in near future at the B factories, the Tevatron and LHCb [3]. Presently only three  $B_c$  states have been experimentally observed out of which masses have been measured only for two low lying states.  $B_c(1S)$  state was discovered in 1998 by the CDF Collaboration in  $p\bar{p}$  collisions at the Fermilab Tevatron and estimated its mass to be  $6.40 \pm 0.39 \pm 0.13$  GeV/ $c^2$  and lifetime to be  $0.46^{+0.18}_{-0.16} \pm 0.03$  ps [4]. Signals consistent with  $B_c^+(2S)$  and  $B_c^{*+}(2S)$  were observed in proton-proton collisions by the CMS Collaboration during the 2015–2018 run at LHC [5]. The mass of the  $B_c^+(2S)$  state was measured to be  $6871.0 \pm 1.2 \pm 0.8 \pm 0.8$  MeV [5]. The mass of  $B_c^{*+}(2S)$  was not measured in this experiment. The vector ground state  $B_c^{*+}(1S)$  has not yet been detected, but the mass difference  $B_c^{*+}(2S) - B_c^{*+}(1S)$  is reported to be 567 MeV [5]. The present PDG masses of  $B_c^+(1S)$  and  $B_c^+(2S)$  states respectively are  $6274.47 \pm 0.27 \pm 0.17$  MeV and  $6871.2 \pm 1.0$  MeV and the mean lifetime of  $B_c^+(1S)$  is estimated to be  $0.510 \pm 0.009$  ps [6].

The  $c\bar{b}$  state cannot annihilate into gluons and are more stable since the flavor quantum numbers are non-vanishing, and these numbers are preserved in electromagnetic and strong interactions. Also, the pseudo-scalar ground state of  $B_c$  meson having energies less than the BD meson production threshold can decay through weak interactions alone, making it a suitable area to examine weak decays [7–9]. Studying the  $B_c$  meson weak decays helps in determining the CKM elements and other Standard Model parameters from the experimental view point [8, 10]. Excited  $B_c$  states below BD threshold can only undergo hadronic or radiative decay to the ground state which will further decay through weak interactions. These are considerably stable as compared to the corresponding  $c\bar{c}$  and  $b\bar{b}$  states [11]. If the mesons possess an energy above the BD threshold, then it is most likely that they will decay into lighter mesons. Higher stability of  $c\bar{b}$  state is the cause for smaller decay widths (few hundred KeV) of  $B_c$  mesons.

Theoretically, there are various approaches employed to study  $c\bar{b}$  systems in literature which include QCD sum rules [12], heavy quark effective theory [13], lattice QCD [14], Bethe-Salpeter equation [9, 15], phenomenological potential models [11, 16], etc. The predictions from these approaches can be validated once further experimental data on these mesons are obtained. In the present article, we have computed the spectra and decay properties of  $B_c$  mesons using a non relativistic potential model. Phenomenological potential model approach is one of the important methods used to investigate heavy meson systems and is very successful [17–25]. Most of the potential models involve solving the non relativistic Schrodinger equation for the chosen  $q\bar{q}$  potential. Since these solutions often cannot be obtained analytically, we need to employ numerical methods. Various numerical methods used in potential models are: approximations based on Runge-Kutta method [25], matrix Numerov method [26], discrete variable representation (DVR) method [27], Fourier grid Hamiltonian method [28], asymptotic iteration method [29], variational method [30], artificial neural network method [31], etc. Among these, the Numerov method is a simple but efficient method to

---

\* Presently at: Centre for High Energy Physics, Indian Institute of Science, Bangalore 560012, India.

† bhaghyesh.mit@manipal.edu; ORCID iD: 0000-0003-3994-9945

solve Schrodinger equation [32]. In this method both the kinetic energy and potential energy are represented as simple matrices on a discretized lattice. Then the problem of solving the Schrodinger equation reduces to solving a matrix eigenvalue problem. The matrix Numerov method have been successfully applied to heavy mesons like charmonium and bottomonium [26]. However, this method has not been applied to open flavored mesons. In this article, we numerically solve the Schrödinger equation for  $B_c$  mesons using the matrix Numerov method.

This article is arranged as follows: in Section II we present the potential model used in our analysis and we also briefly discuss the matrix Numerov method used to solve the Schrodinger equation. The decay properties computed in the present work are given in Section III. Results and discussions of the present work are given in Section IV.

## II. POTENTIAL MODEL

In this work, we have employed a non-relativistic model to study the properties of  $c\bar{b}$  system. Our aim is to solve the nonrelativistic Schrodinger wave equation for the two particle  $c\bar{b}$  system:

$$H\psi = E\psi \quad (1)$$

The model Hamiltonian takes the form

$$H = M + \frac{p^2}{2\mu} + V(r), \quad (2)$$

where  $M = m_c + m_{\bar{b}}$ ,  $p$  is the relative momentum,  $\mu (= m_c m_{\bar{b}} / m_c + m_{\bar{b}})$  is the reduced mass of the  $c\bar{b}$  system, where  $m_c$  and  $m_{\bar{b}}$  are the masses of  $c$  quark and  $\bar{b}$  antiquark respectively. In Eq.2, the quark-antiquark potential  $V(r)$  is taken to be of the following form:

$$V(r) = -\frac{4\alpha_s}{3r} + Ar + B \ln(r\lambda) + \frac{32\pi\alpha_s}{9m_c m_{\bar{b}}} \left( \frac{\sigma}{\sqrt{\pi}} \right)^3 e^{-\sigma^2 r^2} \mathbf{S}_1 \cdot \mathbf{S}_2 \quad (3)$$

The first two terms together in Eq.3 is called the Cornell potential [17, 18, 24] and has been successfully used in quarkonium spectroscopy. The first term of the Cornell potential (generally called the Coulombic term) represents the short distance behaviour and can be derived from the one-gluon-exchange interaction in QCD. The linearly increasing second term models confinement, which is a nonperturbative effect prominent at large inter-quark separation. Even though the specific form of quark-antiquark potential for all distances has not been derived from QCD, various studies [33–37], including Lattice QCD in the static limit [38, 39], indicate the central spin independent QCD potential to be of Cornell type. Using lattice QCD, various authors [40–44] have derived the relativistic corrections to the static potential at order  $1/m$  in the quark mass. In these studies the correction term was found to be proportional to  $\ln(r)$ , where  $r$  is the inter-quark separation. Such logarithmic correction term has also been suggested using effective string theory [45]. This  $\mathcal{O}(1/m)$  correction term has been proved to influence charmonium and bottomonium spectra [42, 43]. Hence, we include this term in our model potential. The last term in Eq.3 represents a Gaussian-smeared contact hyperfine interaction [24]. The spin-hyperfine interaction is treated non-perturbatively in the present analysis. The values of parameters used in our model are given in Table I.

TABLE I. List of parameters.

Parameter	Value	Parameter	Value
$m_c$	1.46 GeV	$m_{\bar{b}}$	4.68 GeV
$A$	0.8126 GeV <sup>2</sup>	$B$	0.0913 GeV
$\lambda$	0.1210 GeV	$\sigma$	3.7374 GeV

The QCD coupling constant  $\alpha_s$  in Eq.3 is computed using the formula

$$\alpha_s(\mu_0^2) = \frac{4\pi}{\left(11 - \frac{2n_f}{3}\right) \ln\left(\frac{\mu_0^2 + M_B^2}{\Lambda^2}\right)},$$

where  $\Lambda (= 0.168 \text{ GeV})$  is the characteristic scale of QCD [46],  $\mu_0 = 2\mu$  with  $\mu$  being the reduced mass,  $n_f (= 4)$  is the number of flavors of quarks having mass lower than  $b$  quark mass,  $M_B (= 1 \text{ GeV})$  is the background mass [47, 48]. The energies and wavefunctions of  $c\bar{b}$  system can be obtained by solving the Schrödinger equation (Eq.1) using the potential given in Eq.3.

In the present article, we have used the matrix Numerov method to numerically solve the Schrodinger equation. In this method [32], the radial coordinate  $r$  is discretized into  $N$  equidistant lattice points  $r_i$ . The kinetic energy operator appearing in the Schrodinger equation is represented by two trigonal matrices and the potential energy operator is a diagonal matrix whose diagonal entries are the values of potential energy evaluated at each lattice point. Thus, the radial Schrodinger equation takes the form of a matrix eigenvalue equation given by [26, 32]

$$-\frac{1}{2\mu}A_{N,N}B_{N,N}^{-1}\psi_i + [V_N(r_i) + \frac{l(l+1)}{2\mu r_i^2} + m_c + m_b]\psi_i = E\psi_i. \quad (4)$$

In Eq.4,  $A$  and  $B$  are  $(N \times N)$  trigonal matrices representing the kinetic energy operator and are given by [26, 32]

$$\begin{aligned} A_{N,N} &= \frac{I_{-1} - 2I_0 + I_1}{d^2} \\ B_{N,N} &= \frac{I_{-1} + 10I_0 + I_1}{12}, \end{aligned} \quad (5)$$

where,  $I_0, I_{-1}, I_1$  are the identity matrix, lower shift identity matrix and upper shift identity matrix respectively, all of order  $N \times N$  and  $d$  is the grid spacing.  $V_N (= V(r_i)\delta_{ij})$  is the  $N \times N$  diagonal potential energy matrix and  $\psi_i = \psi(r_i)$  is an  $N$  dimensional column matrix. The eigenvalue problem corresponding to Eq.4 was solved using Mathematica taking  $N = 350$  and we obtain the bound state eigenvalues ( $E$ ) and values of the corresponding wavefunctions ( $\psi_i$ ) at the chosen grid points. Computed wavefunctions for  $S, P, D$  and  $F$  states are shown in Figure 1.

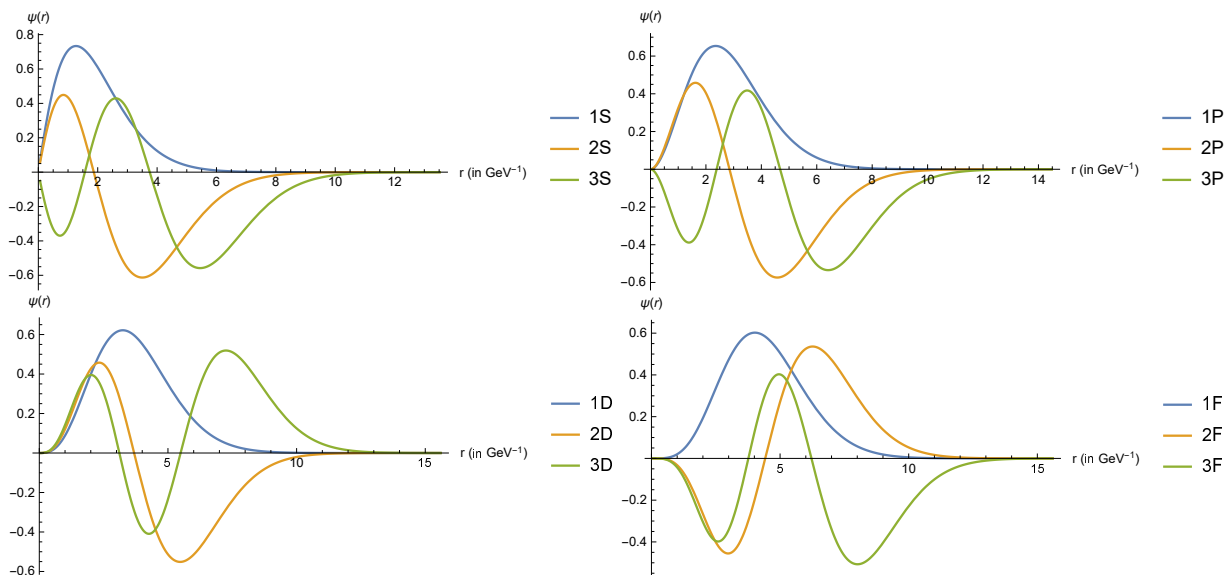


FIG. 1. Wave-functions of first three S-states, P-states, D-states and F-states of  $B_c$  meson

For computing the fine structure of the  $L \neq 0$  states, the spin-orbit and tensor terms are added perturbatively to the obtained eigenvalues. The spin-orbit term chosen is of the form [1, 19, 49]

$$V_{LS}(r) = \frac{4\alpha_s}{3r^3} \left( \frac{1}{m_c} + \frac{1}{m_b} \right) \left( \frac{S_c \cdot L}{m_c} + \frac{S_b \cdot L}{m_b} \right) - \frac{1}{2r} \frac{\partial V^{conf}(r)}{\partial r} \left( \frac{S_c \cdot L}{m_c^2} + \frac{S_b \cdot L}{m_b^2} \right).$$

The tensor term used is of the form [1, 19, 49]

$$V_T = \frac{4}{3} \frac{\alpha_s}{m_c m_b} \frac{1}{r^3} (3S_c \cdot \hat{r} S_b \cdot \hat{r} - S_c \cdot S_b).$$

For mesons with unequal quark masses, the spin-orbit interaction  $V_{LS}$  in the Hamiltonian causes mixing of the  $^1L_J$  and  $^3L_J$  states that have the same  $J^P$  quantum numbers. The physical states are linear combination of these two states. The spin-dependent corrections are evaluated perturbatively in the  $|JM, LS\rangle$  basis [19, 49]. The mass matrix is constructed in this basis and then diagonalized to obtain the mixing eigenstates [49]. The spectra of  $B_c$  mesons obtained from our analysis are listed in Tables II & III. The mixing eigenstates are listed in Table IV. We have also computed the root mean square radii  $\sqrt{\langle r^2 \rangle_{nl}} = \sqrt{\int_0^\infty r^4 |R_{nl}(r)|^2}$  and the results are listed in Table V.

TABLE II. Spectra of  $S$  and  $P$  states (in GeV).

SState	Ours	Exp.[6]	[50]	[19]	[16]	[51]	[52]	[53]	[54]
$B_c(1^1S_0)$	6.273	6.27447±0.00027		6.271	6.272	6.277	6.271	6.272	6.271
$B_c(2^1S_0)$	6.879	6.871±0.001		6.855	6.842	6.845	6.871	6.864	6.855
$B_c(3^1S_0)$	7.303			7.250	7.226	7.284	7.239	7.306	7.220
$B_c(4^1S_0)$	7.658				7.585		7.540	7.684	7.496
$B_c(5^1S_0)$	7.973				7.928		7.805	8.025	7.722
$B_c(6^1S_0)$	8.262						8.046	8.340	
$B_c(1^3S_1)$	6.328		6.331(4)(6)	6.338	6.333	6.288	6.326	6.321	6.338
$B_c(2^3S_1)$	6.912			6.887	6.882	6.853	6.890	6.900	6.886
$B_c(3^3S_1)$	7.330			7.272	7.258	7.290	7.252	7.338	7.240
$B_c(4^3S_1)$	7.681				7.609		7.550	7.714	7.512
$B_c(5^3S_1)$	7.995				7.947		7.813	8.054	7.735
$B_c(6^3S_1)$	8.282						8.054	8.368	
$B_c(1^3P_0)$	6.677		6.712(18)(7)	6.706	6.699	6.639	6.714	6.686	6.701
$B_c(1^3P_2)$	6.751			6.768	6.761	6.667	6.787	6.712	6.773
$B_c(1P')$	6.744			6.750	6.750	6.656	6.776	6.705	6.754
$B_c(1P)$	6.729		6.736(17)(7)	6.741	6.743	6.606	6.757	6.706	6.745
$B_c(2^3P_0)$	7.122			7.122	7.094	7.123	7.107	7.146	7.097
$B_c(2^3P_2)$	7.192			7.164	7.157	7.127	7.160	7.173	7.148
$B_c(2P')$	7.186			7.150	7.147	7.121	7.150	7.165	7.133
$B_c(2P)$	7.168			7.145	7.134	7.088	7.134	7.168	7.125
$B_c(3^3P_0)$	7.489				7.474	7.523	7.420	7.536	7.393
$B_c(3^3P_2)$	7.558				7.524	7.515	7.464	7.565	7.434
$B_c(3P')$	7.551				7.510	7.513	7.458	7.555	7.421
$B_c(3P)$	7.533				7.500	7.488	7.441	7.559	7.414
$B_c(4^3P_0)$	7.813				7.817		7.693	7.885	7.633
$B_c(4^3P_2)$	7.881				7.867		7.732	7.915	7.667
$B_c(4P')$	7.874				7.853		7.727	7.905	7.656
$B_c(4P)$	7.855				7.844		7.710	7.908	7.650

### III. DECAY PROPERTIES

Using the obtained wave functions, we calculate various decay properties of  $B_c$  mesons. The decays of  $c\bar{b}$  states provide important information on heavy quark dynamics and allows us to extract some Standard Model parameters like the CKM elements.

#### A. Decay Constants

Decay constant is an important observable characterising the  $B_c$  meson states [1]. We use the Van-Royen-Weisskopf formula [56] to calculate the decay constant

$$f_{B_c} = \sqrt{\frac{3|R(0)|^2}{\pi M_{B_c}}} = \sqrt{\frac{12|\psi(0)|^2}{M_{B_c}}} \quad (6)$$

The decay constant depends on the radial wave-function at the origin,  $|R(0)|^2$  and on the mass of corresponding  $B_c$  meson,  $M_{B_c}$ . Including the first order QCD correction [57, 58] to the Van-Royen-Weisskopf formula, the expression for decay constant becomes

$$\bar{f}_{B_c} = \sqrt{\frac{3|R(0)|^2}{\pi M_{B_c}}} \left\{ 1 - \frac{\alpha_s}{\pi} \left( \Delta - \frac{m_c - m_{\bar{b}}}{m_c + m_{\bar{b}}} \ln \left| \frac{m_c}{m_{\bar{b}}} \right| \right) \right\} \quad (7)$$

where  $\Delta$  take the values 8/3 for  $^3S_1$  states and 2 for  $^1S_0$  states. Table VI lists  $|R(0)|^2$ , and the decay constants with and without corrections for different  $c\bar{b}$  states.

TABLE III. Spectra of  $D$  and  $F$  states (in GeV).

State	Ours	Exp.[6]	[19]	[16]	[51]	[52]	[53]	[54]
$B_c(1^3D_1)$	7.019		7.028	7.021		7.020	6.998	7.023
$B_c(1^3D_3)$	7.021		7.045	7.029		7.030	6.990	7.042
$B_c(1D')$	7.031		7.036	7.026	6.920	7.032	6.997	7.039
$B_c(1D)$	7.018		7.028	7.025	6.931	7.024	6.994	7.032
$B_c(2^3D_1)$	7.398			7.392		7.336	7.403	7.327
$B_c(2^3D_3)$	7.404			7.405		7.348	7.399	7.344
$B_c(2D')$	7.409			7.400	7.345	7.347	7.403	7.340
$B_c(2D)$	7.401			7.399	7.334	7.343	7.401	7.335
$B_c(3^3D_1)$	7.730			7.732		7.611	7.762	7.573
$B_c(3^3D_3)$	7.739			7.750		7.625	7.761	7.589
$B_c(3D')$	7.741			7.743	7.704	7.623	7.764	7.584
$B_c(3D)$	7.736			7.741	7.694	7.620	7.762	7.581
$B_c(1^3F_2)$	7.269		7.269	7.273		7.235	7.234	7.252
$B_c(1^3F_4)$	7.251		7.271	7.277		7.227	7.244	7.253
$B_c(1F')$	7.273		7.266	7.269		7.240	7.242	7.260
$B_c(1F)$	7.251		7.276	7.268		7.224	7.241	7.248
$B_c(2^3F_2)$	7.611			7.618		7.518	7.607	7.507
$B_c(2^3F_4)$	7.598			7.617		7.514	7.617	7.510
$B_c(2F')$	7.616			7.616		7.525	7.615	7.514
$B_c(2F)$	7.597			7.615		7.508	7.614	7.505
$B_c(3^3F_2)$	7.920					7.730	7.946	
$B_c(3^3F_4)$	7.910					7.771	7.956	
$B_c(3F')$	7.925					7.779	7.954	
$B_c(3F)$	7.909					7.768	7.953	

TABLE IV. Mixing eigenstates.

State	Multiplet	State	Multiplet
$1P'$	$-0.728916  1^1P_1\rangle - 0.684603  1^3P_1\rangle$	$2D'$	$-0.55469  1^1D_2\rangle + 0.832057  1^3D_2\rangle$
$1P$	$0.684603  1^1P_1\rangle - 0.728916  1^3P_1\rangle$	$2D$	$-0.832057  1^1D_2\rangle - 0.55469  1^3D_2\rangle$
$2P'$	$-0.746111  2^1P_1\rangle + 0.665822  2^3P_1\rangle$	$3D'$	$-0.524727  1^1D_2\rangle + 0.851271  1^3D_2\rangle$
$2P$	$-0.665822  2^1P_1\rangle - 0.746111  2^3P_1\rangle$	$3D$	$-0.851271  1^1D_2\rangle - 0.524727  1^3D_2\rangle$
$3P'$	$-0.75317  3^1P_1\rangle - 0.657826  3^3P_1\rangle$	$1F'$	$0.63315  1^1F_3\rangle + 0.774029  1^3F_3\rangle$
$3P$	$0.657826  3^1P_1\rangle - 0.75317  3^3P_1\rangle$	$1F$	$-0.774029  1^1F_3\rangle + 0.63315  1^3F_3\rangle$
$4P'$	$-0.756891  4^1P_1\rangle + 0.653541  4^3P_1\rangle$	$2F'$	$-0.631225  1^1F_3\rangle + 0.7756  1^3F_3\rangle$
$4P$	$-0.653541  4^1P_1\rangle - 0.756891  4^3P_1\rangle$	$2F$	$-0.7756  1^1F_3\rangle - 0.631225  1^3F_3\rangle$
$1D'$	$-0.574781  1^1D_2\rangle + 0.818308  1^3D_2\rangle$	$3F'$	$-0.629269  1^1F_3\rangle + 0.777187  1^3F_3\rangle$
$1D$	$-0.818308  1^1D_2\rangle - 0.574781  1^3D_2\rangle$	$3F$	$-0.777187  1^1F_3\rangle - 0.629269  1^3F_3\rangle$

## B. Weak Decays

We have analysed the weak decays of the low lying pseudoscalar states using a widely studied model called the spectator model [1, 8, 64]. According to this model, the decay width of  $B_c$  mesons is obtained as a result of three major processes: a)  $c$ -quark decay with  $b$ -antiquark as spectator, b)  $b$ -antiquark decay with  $c$ -quark as spectator and c) the annihilation decay of  $c\bar{b}$  meson. These processes are represented [1] in Figure 2.

During the decay,  $c$ -quark can decay into strange ( $s$ ) or down ( $d$ ) quark and simultaneously also decay into lepton-neutrino pair through the exchange of  $W^+$  boson. Similarly  $b$ -antiquark decays into either charm ( $c$ ) or up ( $u$ ) quark and simultaneously into lepton-neutrino pair with the exchange of  $W^+$  boson. The annihilation process of  $B_c$  meson yields a quark-antiquark pair or a lepton-neutrino pair, ie.,  $B_c^+ \rightarrow l^+\nu_l, (c\bar{s}, u\bar{s})$  where  $l = e, \mu, \tau$  [65]. The decay width for each of these three process can be calculated using the following formulae:

$$\Gamma(c \rightarrow X) = \frac{5G_F^2 |V_{cs}|^2 m_c^5}{192\pi^3}$$

$$\Gamma(b \rightarrow X) = \frac{9G_F^2 |V_{cb}|^2 m_b^5}{192\pi^3}$$

TABLE V. RMS radii of  $B_c$  meson states (in fm).

State	Ours	[16]	[55]
$B_c(1^1 S_0)$	0.32	0.33	0.318
$B_c(2^1 S_0)$	0.68	0.63	0.723
$B_c(3^1 S_0)$	0.97	0.87	1.052
$B_c(4^1 S_0)$	1.22	1.05	1.337
$B_c(5^1 S_0)$	1.45	1.21	
$B_c(6^1 S_0)$	1.66		
$B_c(1^3 S_1)$	0.35		0.334
$B_c(2^3 S_1)$	0.70		0.732
$B_c(3^3 S_1)$	0.98		1.059
$B_c(4^3 S_1)$	1.24		1.342
$B_c(5^3 S_1)$	1.46		
$B_c(6^3 S_1)$	1.68		
$B_c(1P)$	0.55	0.53	0.562
$B_c(2P)$	0.86	0.79	0.920
$B_c(3P)$	1.12	0.99	1.220
$B_c(4P)$	1.36	1.16	
$B_c(1D)$	0.71	0.67	0.752
$B_c(2D)$	1.00	0.90	1.083
$B_c(3D)$	1.25	1.08	1.364
$B_c(1F)$	0.86		
$B_c(2F)$	1.13		
$B_c(3F)$	1.37		

TABLE VI. Radial wave function at origin (in  $\text{GeV}^3$ ) and decay constants (in  $\text{GeV}$ ).

State	$ R(0) ^2$	[59]	$f_{B_c}$	$\bar{f}_{B_c}$	[59]	[53]	[60]	[61]	[62][63]
$B_c(1^1 S_0)$	2.835	2.2393	0.657	0.535	0.484	0.433	0.439(30)(17)	523(62)	528
$B_c(2^1 S_0)$	1.662	1.2606	0.480	0.391	0.347	0.355	0.282(13)(10)		
$B_c(3^1 S_0)$	1.357	1.0399	0.421	0.343	0.306	0.326	0.237(6)(14)		
$B_c(4^1 S_0)$	1.204	0.9358	0.387	0.316	0.284	0.307			
$B_c(5^1 S_0)$	1.108	0.8726	0.364	0.297	0.269	0.294			
$B_c(6^1 S_0)$	1.040	0.8293	0.347	0.283	0.258	0.284			
$B_c(1^3 S_1)$	1.352	1.9566	0.452	0.368	0.405	0.435	0.417(51)(27)	474(42)	384
$B_c(2^3 S_1)$	0.898	1.2018	0.352	0.287	0.304	0.356	0.297(35)(3)		
$B_c(3^3 S_1)$	0.772	1.0083	0.317	0.258	0.270	0.326	0.257(29)(5)		
$B_c(4^3 S_1)$	0.709	0.9138	0.297	0.242	0.251	0.308			
$B_c(5^3 S_1)$	0.671	0.8553	0.283	0.231	0.239	0.295			
$B_c(6^3 S_1)$	0.643	0.8148	0.272	0.222	0.229	0.285			

$$\Gamma(ann) = \sum_i \frac{G_F^2}{8\pi} |V_{cb}|^2 f_{B_c}^2 M_{B_c} m_i^2 \left(1 - \frac{m_i^2}{M_{B_c}^2}\right) C_i \quad (8)$$

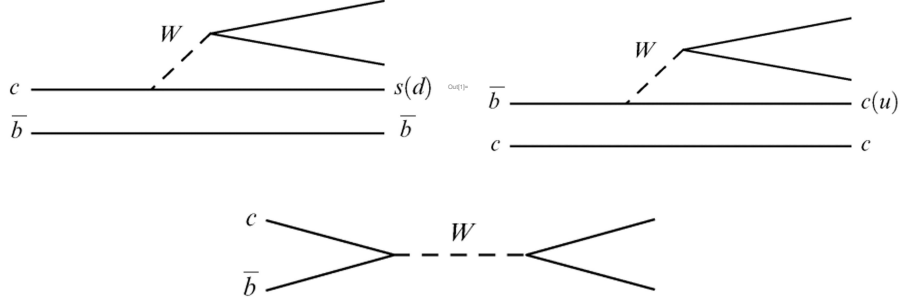
In the above equations, the values of the Cabibo-Kobayashi-Maskawa (CKM) matrix elements  $|V_{cs}| = 0.975$  and  $|V_{cb}| = 0.0408$  are taken from PDG [6].  $G_f = 1.1663788 \times 10^{-5} \text{ GeV}^{-2}$  is the Fermi constant [6]. For annihilation decay, we have considered two main channels, that is  $c\bar{s}$  and  $\tau\nu_\tau$ . In Eq.8,  $C_i = 3 |V_{cs}|^2$  for  $c\bar{s}$  channel and  $C_i = 1$  for  $\tau\nu_\tau$  channel [1]. These formulae do not take into account the quark binding effects [1, 9]. The total decay width can be written as the sum of decay widths for all the three processes [1]:

$$\Gamma(B_c \rightarrow X) = \Gamma(b \rightarrow X) + \Gamma(c \rightarrow X) + \Gamma(ann)$$

The decay lifetime ( $\tau$ ) is then given by

$$\tau = \frac{\hbar}{\Gamma},$$

where  $\hbar = 6.582 \times 10^{-25} \text{ GeV}\cdot\text{sec}$ . The lifetime directly depends on the decay modes. The branching ratio ( $\mathcal{B}$ ) is the probability of decay through a particular channel. The branching ratios for  $c$ -decay,

FIG. 2.  $c$ -quark decay,  $b$ -antiquark decay and annihilation of  $B_c$  mesons

$\bar{b}$ -decay and decay due to annihilation is calculated by dividing the decay width corresponding to a particular process by the total decay width:

$$\begin{aligned}\mathcal{B}(c \rightarrow X) &= \frac{\Gamma(c \rightarrow X)}{\Gamma(B_c \rightarrow X)} \\ \mathcal{B}(b \rightarrow X) &= \frac{\Gamma(b \rightarrow X)}{\Gamma(B_c \rightarrow X)} \\ \mathcal{B}(ann) &= \frac{\Gamma(ann)}{\Gamma(B_c \rightarrow X)}\end{aligned}\quad (9)$$

The results obtained for the annihilation decay widths and total decay widths for two different channels and the corresponding lifetimes and branching ratios are listed down in Table VII. Here, the branching ratios for Refs. [9], [66] and [30] have been evaluated by using their corresponding  $\Gamma$  values using Eqns. 9.

TABLE VII. Comparison of weak partial decay and annihilation widths (in  $10^{-3}$  eV), total width (in  $10^{-3}$  eV), lifetime (in ps) and branching ratios.

	$\Gamma(c \rightarrow X)$	$\Gamma(b \rightarrow X)$	$\Gamma(ann)$	$\Gamma(B_c \rightarrow X)$	$\tau$	$\mathcal{B}(c \rightarrow X)$	$\mathcal{B}(b \rightarrow X)$	$\mathcal{B}(ann)$
ours	0.72	0.77	0.13	1.62	0.41	0.44	0.47	0.08
Exp. [6]					$0.510 \pm 0.009$			
[9]	0.51	0.75	0.14	1.40	0.47	0.36	0.54	0.10
[19]	0.33	0.48	0.067	0.88	0.75	0.38	0.54	0.08
[66]	0.8958	1.0410	0.0057	1.9425	0.339	0.461	0.536	0.003
[30]	0.875	0.419	0.0923	1.3863	0.47	0.63	0.30	0.07

### C. Radiative decays

The electric dipole (E1) and magnetic dipole (M1) radiative transitions that appears from the multipole expansions help us understand the  $c\bar{b}$  system better. The  $B_c$  mesons below the BD threshold can undergo radiative decay to the ground state which further decays through weak interactions. In E1 transitions  $\Delta S = 0$  and  $|\Delta L| = 1$ . The partial decay widths due to E1 transitions are calculated using [19]

$$\Gamma_{E1}(i \rightarrow f\gamma) = \frac{4\alpha\langle e_Q \rangle^2 \omega^3}{3} |\langle f | r | i \rangle|^2 C_{fi} \delta_{SS'},$$

where  $i$  ( $\equiv n^{2S+1}L_J$ ) is the initial state and  $f$  ( $\equiv n'^{2S'+1}L_{J'}$ ) is the final state,  $\langle e_Q \rangle = \frac{m_{\bar{b}}e_c - m_c e_{\bar{b}}}{m_b + m_c}$  is the mean charge with  $e_c = \frac{2}{3}$  and  $e_{\bar{b}} = \frac{1}{3}$  being the charges of  $c$ -quark and  $b$ -antiquark respectively. The photon energy  $\omega = \frac{M_i^2 - M_f^2}{2M_i}$ , where  $M_i$  and  $M_f$  are the masses of the initial and final states.  $\alpha$  is the fine structure constant,  $\langle f | r | i \rangle$  is the transition matrix element and  $C_{fi}$  is the statistical factor which is calculated using the 6J symbol, with  $S = S_i = S_f$ , as

$$C_{fi} = \max(L_i, L_f)(2J_f + 1) \left\{ \begin{matrix} L_f & J_f & S \\ J_i & L_i & 1 \end{matrix} \right\}^2$$

In M1 transitions  $|\Delta L| = 0$ . Partial decay widths for M1 transitions are calculated using [19]

$$\Gamma_{M1}(i \rightarrow f\gamma) = \frac{\alpha\mu^2\omega^3}{3} (2J_f + 1) |\langle f | j_0(\omega r/2) | i \rangle|^2,$$

where  $\alpha$  is the fine structure constant,  $j_0(\omega r/2)$  is zeroth spherical Bessel function and  $\mu = \frac{m_b c - m_c c}{4m_b m_c}$  is the magnetic dipole moment.

Tables VIII - XIV gives the  $E1$  and  $M1$  radiative decay widths along with the photon energies (in GeV) and absolute value of the transition matrix elements (in  $\text{GeV}^{-1}$ ).

TABLE VIII. E1 radiative decay widths (in keV) of  $n = 1$ ,  $L = 1, 2$  states.

$i$	$f$	$i \rightarrow f$	$\omega$	$\langle f r i \rangle$	$\Gamma_{E1}$	[52]	[19]	[46]	[67]
$1^3P_0$	$1^3S_1$	$1^3P_0 \rightarrow 1^3S_1$	0.340	-1.760	72	96	55	67.2	58.55
$1^3P_2$	$1^3S_1$	$1^3P_2 \rightarrow 1^3S_1$	0.409	-1.760	127	87	83	107	64.24
$1P_1'$	$1^3S_1$	$1^3P_1 \rightarrow 1^3S_1$	0.403	-1.760	57	40	11	13.6	9.98
	$1^1S_0$	$1^1P_1 \rightarrow 1^1S_0$	0.454	-1.605	77	74	80	132	72.28
$1P_1$	$1^3S_1$	$1^3P_1 \rightarrow 1^3S_1$	0.389	-1.760	58	70	60	78.9	51.14
	$1^1S_0$	$1^1P_1 \rightarrow 1^1S_0$	0.440	-1.605	61	35	13	18.4	13.70
$1^3D_1$	$1^3P_0$	$1^3D_1 \rightarrow 1^3P_0$	0.334	2.779	114	65	55	128	57.76
	$1^3P_2$	$1^3D_1 \rightarrow 1^3P_2$	0.264	2.779	2.8	0.7	1.8	5.52	2.15
	$1P_1'$	$1^3D_1 \rightarrow 1^3P_1$	0.270	2.779	21	12	4.4	7.66	5.55
	$1P_1$	$1^3D_1 \rightarrow 1^3P_1$	0.285	2.779	28	29	28	73.8	29.61
$1^3D_3$	$1^3P_2$	$1^3D_3 \rightarrow 1^3P_2$	0.264	2.779	103	67	78	102	73.98
$1D_2'$	$1^3P_2$	$1^3D_2 \rightarrow 1^3P_2$	0.274	2.779	19	8.3	8.8	12.8	20.57
	$1P_1'$	$1^3D_2 \rightarrow 1^3P_1$	0.281	2.779	100	41	63	116	
	$1P_1$	$1^3D_2 \rightarrow 1^3P_1$	0.295	2.779	2.2	0.39	7.0	7.25	
$1D_2$	$1^3P_2$	$1^3D_2 \rightarrow 1^3P_2$	0.263	2.779	8.3	8.7	9.6	27.5	18.17
	$1P_1'$	$1^1D_2 \rightarrow 1^1P_1$	0.269	-2.775	7.0	1.09	15	14.1	
	$1P_1$	$1^1D_2 \rightarrow 1^1P_1$	0.284	-2.775	107	44	64	112	

TABLE IX. E1 radiative decay widths (in keV) of  $n = 1$ ,  $L = 3$  states.

$i$	$f$	$i \rightarrow f$	$\omega$	$\langle f r i \rangle$	$\Gamma_{E1}$	[52]	[19]
$1^3F_2$	$1^3D_1$	$1^3F_2 \rightarrow 1^3D_1$	0.245	3.621	125	78	75
	$1^3D_3$	$1^3F_2 \rightarrow 1^3D_3$	0.244	3.621	0.65	0.12	0.4
	$1D_2'$	$1^3F_2 \rightarrow 1^3D_2$	0.234	3.621	13	5.72	6.3
	$1D_2$	$1^3F_2 \rightarrow 1^3D_2$	0.246	3.621	7.7	6.36	6.5
$1^3F_4$	$1^3D_3$	$1^3F_4 \rightarrow 1^3D_3$	0.227	3.621	117	69	81
$1F_3'$	$1^3D_3$	$1^3F_3 \rightarrow 1^3D_3$	0.248	3.621	10	4.76	3.7
	$1D_2'$	$1^3F_3 \rightarrow 1^3D_2$	0.238	3.621	126	32	78
	$1D_2$	$1^3F_3 \rightarrow 1^3D_2$	0.250	3.621	1.5	0.04	0.5
$1F_3$	$1^3D_3$	$1^3F_3 \rightarrow 1^3D_3$	0.226	3.621	5.2	4.91	5.4
	$1D_2'$	$1^1F_3 \rightarrow 1^1D_2$	0.217	-3.621	0.19	0.22	0.04
	$1D_2$	$1^1F_3 \rightarrow 1^1D_2$	0.229	-3.621	114	29	82

#### IV. DISCUSSION AND CONCLUSION

In this work we have used the matrix Numerov method to solve the Schrodinger equation for  $B_c$  mesons. The model potential consists of the familiar Cornell potential along with an  $\mathcal{O}(1/m)$  correction from LQCD. The hyperfine interaction term has been considered non-perturbatively in our analysis. We have solved the matrix eigenvalue problem and computed the spectra of  $S$ ,  $P$ ,  $D$  and  $F$  wave states and their corresponding wave functions. The masses are presented in Tables II and III in comparison with some relativistic [19, 54] and nonrelativistic [52, 53] potential models. In Ref.[51],  $Bc$  spectra has been obtained using the Tamm-Dancoff approximation. The masses obtained in the present work are comparable with the predictions from other theoretical studies. Also our masses for  $Bc(1^3S_1)$ ,



TABLE X. E1 radiative decay widths (in keV) of  $n = 2$ ,  $L = 0, 1$  states.

$i$	$f$	$i \rightarrow f$	$\omega$	$\langle f r i \rangle$	$\Gamma_{E1}$	[52]	[19]	[46]	[67]
$2^3S_1$	$1^3P_0$	$2^3S_1 \rightarrow 1^3P_0$	0.231	2.166	12	3.48	2.9	3.78	0.94
	$1^3P_2$	$2^3S_1 \rightarrow 1^3P_2$	0.160	2.166	19	6.98	5.7	5.18	2.28
	$1P'_1$	$2^3S_1 \rightarrow 1^3P_1$	0.166	2.166	6.0	1.56	0.7	0.63	0.26
	$1P_1$	$2^3S_1 \rightarrow 1^3P_1$	0.181	2.166	8.8	4.62	4.7	5.05	1.45
$2^1S_0$	$1P'_1$	$2^1S_0 \rightarrow 1^1P_1$	0.134	2.276	12	6.38	6.1	3.72	3.03
	$1P_1$	$2^1S_0 \rightarrow 1^1P_1$	0.149	2.276	14	5.33	1.3	1.02	0.62
$2^3P_0$	$2^3S_1$	$2^3P_0 \rightarrow 2^3S_1$	0.207	2.792	41	53	42	29.2	55.05
	$1^3S_1$	$2^3P_0 \rightarrow 1^3S_1$	0.750	0.258	17	41	1.0		
	$1^3D_1$	$2^3P_0 \rightarrow 1^3D_1$	0.102	2.333	6.9	5.6	4.2	0.036	3.94
$2^3P_2$	$2^3S_1$	$2^3P_2 \rightarrow 2^3S_1$	0.274	2.792	96	50	55	57.3	64.92
	$1^3S_1$	$2^3P_2 \rightarrow 1^3S_1$	0.812	0.258	21	52	14		
	$1^3D_1$	$2^3P_2 \rightarrow 1^3D_1$	0.170	2.333	0.3	0.13	0.1	0.035	0.07
	$1^3D_3$	$2^3P_2 \rightarrow 1^3D_3$	0.169	2.333	26	14	6.8	1.59	6.28
	$1D'_2$	$2^3P_2 \rightarrow 1^3D_2$	0.159	2.333	2.6	0.93	0.7	0.113	0.91
	$1D_2$	$2^3P_2 \rightarrow 1^3D_2$	0.172	2.333	1.6	1.1	0.6	0.269	1.16
	$2P'_1$	$2^3P_1 \rightarrow 2^3S_1$	0.268	2.792	40	25	5.5	9.07	15.11
$2P_1$	$1^3S_1$	$2^3P_1 \rightarrow 1^3S_1$	0.806	0.258	9.2	26	0.6		
	$2^1S_0$	$2^1P_1 \rightarrow 2^1S_0$	0.300	-2.539	58	36	52	72.5	56.28
	$1^1S_0$	$2^1P_1 \rightarrow 1^1S_0$	0.854	-0.318	21	44	19		
	$1^3D_1$	$2^3P_1 \rightarrow 1^3D_1$	0.164	2.333	3.2	1.27	0.2	0.073	0.35
	$1D'_2$	$2^3P_1 \rightarrow 1^3D_2$	0.153	2.333	19	1.05	5.5	1.20	
	$1D_2$	$2^3P_1 \rightarrow 1^3D_2$	0.165	2.338	2.3	0.03	1.3	0.149	
	$2^3S_1$	$2^3P_1 \rightarrow 2^3S_1$	0.252	2.792	41	34	45	37.9	50.40
	$1^3S_1$	$2^3P_1 \rightarrow 1^3S_1$	0.791	0.258	11	40	5.4		
	$2^1S_0$	$2^1P_1 \rightarrow 2^1S_0$	0.283	-2.539	39	19	5.7	11.7	16.52
	$1^1S_0$	$2^1P_1 \rightarrow 1^1S_0$	0.839	-0.318	16	25	2.1		
$1^3D_1$	$2^3P_1 \rightarrow 1^3D_1$	0.148	2.333	3.0	1.45	1.6	0.184	1.14	
$1D'_2$	$2^3P_1 \rightarrow 1^3D_2$	0.136	2.333	0.3	0.006	0.8	0.021		
$1D_2$	$2^3P_1 \rightarrow 1^3D_2$	0.149	2.338	18	0.84	3.6	0.418		

$Bc(1^3P_0)$  and  $Bc(1P)$  states are good in agreement with the lattice results [50]. From our results, we obtain the mass difference  $B_c^{*+}(2S) - B_c^{*+}(1S)$  to be 584 MeV which is close to the experimental difference of 567 MeV [5]. Presently, a thorough analysis of the spectra cannot be done due to lack of experimental data.

Table V gives the rms radii of  $Bc$  mesons for various radial and orbital excitations. We see that vector mesons have slightly higher rms radii than the corresponding pseudoscalar mesons. Furthermore, the rms radii increases with increase in radial and orbital quantum numbers. Charmonium [27, 70] and bottomonium [26, 71] systems also exhibit similar trend in rms radii. Our results for decay constants are consistent with results from nonrelativistic models [53, 59, 60] and other theoretical approaches like light front formalism [61] and QCD sum rules [62, 63]. From Table VI we see that  $f_v < f_p$  and the decay constants decreases with increase in radial quantum number. Thus, we see that while the rms radii increases and decay constants decreases as the radial quantum number increases. This trend as suggested in Ref.[61] may be due to the fact that as radial quantum number increases, the mesons are loosely bound and hence a larger spread in radial distribution. Similar trend is also seen in charmonium and bottomonium systems.

We have calculated weak decay widths and lifetimes following the spectator model. The weak decay widths, branching ratios and lifetimes for  $1^1S_0$  state are listed in Table VII. We see that the branching ratio for  $b$  quark decay is greater than that for  $c$  quark decay and annihilation decay. This result is in agreement with the predictions from other models. Knowing the lifetime of the particle helps us understand the weak interaction properties. The obtained lifetime of the pseudoscalar  $1^1S_0$  state is 0.41 ps which is comparable with the experimental lifetime of  $0.510 \pm 0.009$  ps [6].

The decay widths for radiative E1 transitions for ground and various radially and orbitally excited states are given in Tables VIII-XII along with the photon energies and the overlap integrals. The decay widths are also compared with the predictions from other models and our results are in reasonable agreement with these models. The M1 radiative widths of lower and higher  $S$  wave states are given in Tables XIII and XIV along with the photon energies and the overlap integrals. We have compared the widths with other relativistic and nonrelativistic models. In the nonrelativistic limit, the transitions for which the radial quantum number ( $n$ ) changes are hindered because of the wavefunction orthogonality. However, from our results, we see that these hindered transitions have widths comparable

TABLE XI. E1 radiative decay widths (in keV) of  $n = 2$ ,  $L = 2$  states.

$i$	$f$	$i \rightarrow f$	$\omega$	$\langle f r i \rangle$	$\Gamma_{E1}$	[52]	
$2^3D_1$	$2^3P_0$	$2^3D_1 \rightarrow 2^3P_0$	0.271	-3.674	107	46	
	$1^3P_0$	$2^3D_1 \rightarrow 1^3P_0$	0.686	0.24	7.4	41.8	
	$2^3P_2$	$2^3D_1 \rightarrow 2^3P_2$	0.203	-3.674	2.2	0.58	
	$1^3P_2$	$2^3D_1 \rightarrow 1^3P_2$	0.619	0.24	0.3	8.13	
	$2P'_1$	$2^3D_1 \rightarrow 2^3P_1$	0.209	-3.674	16	10.15	
	$1P'_1$	$2^3D_1 \rightarrow 1^3P_1$	0.625	0.24	2.0	7.6	
	$2P_1$	$2^3D_1 \rightarrow 2^3P_1$	0.226	-3.674	26	20.88	
	$1P_1$	$2^3D_1 \rightarrow 1^3P_1$	0.639	0.24	2.4	12.5	
	$1^3F_2$	$2^3D_1 \rightarrow 1^3F_2$	0.128	-2.449	3.8		
	$2^3D_3$	$2^3P_2$	$2^3D_3 \rightarrow 2^3P_2$	0.209	-3.674	88	54
$1^3P_2$		$2^3D_3 \rightarrow 1^3P_2$	0.624	0.24	10	32	
$1^3F_2$		$2^3D_3 \rightarrow 1^3F_2$	0.133	-2.449	1.2		
$1^3F_4$		$2^3D_3 \rightarrow 1^3F_4$	0.151	-2.449	13		
$1F'_3$		$2^3D_3 \rightarrow 1^3F_3$	0.129	-2.449	3.0		
$1F_3$		$2^3D_3 \rightarrow 1^3F_3$	0.152	-2.449	3.2		
$2D'_2$		$2^3P_2$	$2^3D_2 \rightarrow 2^3P_1$	0.214	-3.674	16	6.71
	$1^3P_2$	$2^3D_2 \rightarrow 1^3P_1$	0.629	0.24	1.8	7.28	
	$2P'_1$	$2^3D_2 \rightarrow 2^3P_1$	0.220	-3.674	82	29	
	$2P_1$	$2^1D_2 \rightarrow 2^1P_1$	0.237	-3.664	3.7	0.24	
	$1P'_1$	$2^3D_2 \rightarrow 1^3P_1$	0.635	0.24	8.6	19	
	$1P_1$	$2^1D_2 \rightarrow 1^1P_1$	0.649	-0.243	0.2	1.48	
	$1F'_3$	$2^3D_2 \rightarrow 1^3F_3$	0.135	2.449	8.9		
	$1F_3$	$2^1D_2 \rightarrow 1^1F_3$	0.157	-2.449	0.1		
	$2D_2$	$2^3P_2$	$2^3D_2 \rightarrow 2^3P_2$	0.206	-3.674	6.5	6.33
		$1^3P_2$	$2^3D_2 \rightarrow 1^3P_2$	0.622	0.24	0.8	7.04
$2P'_1$		$2^3D_2 \rightarrow 2^3P_1$	0.212	-3.674	8.3	0.74	
$2P_1$		$2^1D_2 \rightarrow 2^1P_1$	0.229	-3.664	96	34	
$1P'_1$		$2^3D_2 \rightarrow 1^3P_1$	0.628	0.24	0.8	0.12	
$1P_1$		$2^1D_2 \rightarrow 1^1P_1$	0.642	-0.243	9.3	22.6	
$1F'_3$		$2^3D_2 \rightarrow 1^3F_3$	0.127	2.449	0.6		
$1F_3$		$2^1D_2 \rightarrow 1^1F_3$	0.149	-2.449	15		

TABLE XII. E1 radiative decay widths (in keV) of  $n = 2$ ,  $L = 3$  states.

$i$	$f$	$i \rightarrow f$	$\omega$	$\langle f r i \rangle$	$\Gamma_{E1}$
$2^3F_2$	$1^3D_1$	$2^3F_2 \rightarrow 1^3D_1$	0.245	3.621	125
	$1^3D_3$	$2^3F_2 \rightarrow 1^3D_3$	0.244	3.621	0.6
	$1D'_2$	$2^3F_2 \rightarrow 1^3D_2$	0.234	3.621	14
	$1D_2$	$2^3F_2 \rightarrow 1^3D_2$	0.246	3.621	7.7
$2^3F_4$	$1^3D_3$	$2^3F_4 \rightarrow 1^3D_3$	0.227	3.621	117
$2F'_3$	$1^3D_3$	$2^3F_3 \rightarrow 1^3D_3$	0.248	3.621	10
	$1D'_2$	$2^3F_3 \rightarrow 1^3D_2$	0.238	3.621	126
	$1D_2$	$2^3F_3 \rightarrow 1^3D_2$	0.25	-3.621	1.5
$2F_3$	$1^3D_3$	$2^3F_3 \rightarrow 1^3D_3$	0.226	3.621	5.2
	$1D'_2$	$2^1F_3 \rightarrow 1^1D_2$	0.217	3.621	0.2
	$1D_2$	$2^1F_3 \rightarrow 1^1D_2$	0.229	-3.621	115

to the allowed transitions. In our model, we have treated the spin-spin interaction non-perturbatively, and hence the singlet and triplet states for the same  $n$  will have slightly different wavefunctions. As a result, the wavefunction orthogonality will be broken as suggested in Ref.[19]. Another reason for the appreciable widths of the hindered transitions is the large  $\omega^3$  dependence of the M1 decay width.

To sum up, the current article applied the matrix Numerov method to study the spectra and decay properties of  $B_c$  mesons. The findings of this study are consistent with both available experimental data and predictions from other theoretical frameworks.

TABLE XIII. M1 radiative decay widths (in eV) of  $n = 1, 2, 3$ ,  $L = 0$  states.

$i \rightarrow f$	$\omega$	$\langle i   \dots   f \rangle$	$\Gamma_{M1}$	[52]	[19]	[55]	[68]	[46]	[69]	[53]
$1^3S_1 \rightarrow 1^1S_0\gamma$	0.054	-0.383	57	57	80	27	52	33	18.9	53.109
$2^3S_1 \rightarrow 2^1S_0\gamma$	0.033	-0.382	12	2.4	10	0.0016	10	17	3.7	21.119
$2^3S_1 \rightarrow 1^1S_0\gamma$	0.609	-0.061	2042	1205	600	367	650	428	135.7	481.572
$2^1S_0 \rightarrow 1^3S_1\gamma$	0.529	-0.008	64	99	300	6	250	488	163.8	568.346
$3^3S_1 \rightarrow 3^1S_0\gamma$	0.026	0.382	6.6	0.8	3	0.32				
$3^3S_1 \rightarrow 2^1S_0\gamma$	0.436	0.072	1043	356	200	96				
$3^3S_1 \rightarrow 1^1S_0\gamma$	0.980	0.041	3831	1885	600	431				
$3^1S_0 \rightarrow 2^3S_1\gamma$	0.380	-0.020	166	152	60	4.6				
$3^1S_0 \rightarrow 1^3S_1\gamma$	0.910	-0.008	400	510	4200	0.646				

TABLE XIV. M1 radiative decay widths (in eV) of  $n = 4, 5$ ,  $L = 0$  states.

$i \rightarrow f$	$\omega$	$\langle i   \dots   f \rangle$	$\Gamma_{E1}$	[52]	$i \rightarrow f$	$\omega$	$\langle i   \dots   f \rangle$	$\Gamma_{M1}$	[52]
$4^3S_1 \rightarrow 4^1S_0\gamma$	0.023	-0.381	4.5	0.35	$5^1S_0 \rightarrow 2^3S_1\gamma$	0.990	-0.017	2116	1260
$4^3S_1 \rightarrow 3^1S_0\gamma$	0.369	-0.081	805	252	$5^1S_0 \rightarrow 1^3S_1\gamma$	1.475	-0.009	1967	1893
$4^3S_1 \rightarrow 2^1S_0\gamma$	0.760	-0.049	2548	806	$6^3S_1 \rightarrow 6^1S_0\gamma$	0.020	-0.381	2.8	0.18
$4^3S_1 \rightarrow 1^1S_0\gamma$	1.279	-0.033	5644	2501	$6^3S_1 \rightarrow 5^1S_0\gamma$	0.303	-0.095	611	191
$4^1S_0 \rightarrow 3^3S_1\gamma$	0.321	0.030	225	186	$6^3S_1 \rightarrow 4^1S_0\gamma$	0.600	-0.063	2100	643
$4^1S_0 \rightarrow 2^3S_1\gamma$	0.709	-0.018	833	579	$6^3S_1 \rightarrow 3^1S_0\gamma$	0.921	-0.047	4181	1239
$4^1S_0 \rightarrow 1^3S_1\gamma$	1.214	-0.009	1023	1122	$6^3S_1 \rightarrow 2^1S_0\gamma$	1.284	-0.035	6490	1917
$5^3S_1 \rightarrow 5^1S_0\gamma$	0.021	-0.381	3.4	0.18	$6^3S_1 \rightarrow 1^1S_0\gamma$	1.765	-0.027	9625	3772
$5^3S_1 \rightarrow 4^1S_0\gamma$	0.329	-0.089	687	210	$6^1S_0 \rightarrow 5^3S_1\gamma$	0.263	-0.047	291	225
$5^3S_1 \rightarrow 3^1S_0\gamma$	0.661	-0.057	2257	675	$6^1S_0 \rightarrow 4^3S_1\gamma$	0.560	-0.034	1488	849
$5^3S_1 \rightarrow 2^1S_0\gamma$	1.037	-0.040	4372	1316	$6^1S_0 \rightarrow 3^3S_1\gamma$	0.879	0.025	3141	1613
$5^3S_1 \rightarrow 1^1S_0\gamma$	1.536	-0.029	7564	3107	$6^1S_0 \rightarrow 2^3S_1\gamma$	1.239	-0.017	4127	2203
$5^1S_0 \rightarrow 4^3S_1\gamma$	0.286	-0.039	264	209	$6^1S_0 \rightarrow 1^3S_1\gamma$	1.707	-0.009	3272	2822
$5^1S_0 \rightarrow 3^3S_1\gamma$	0.617	0.026	1194	720					

## REFERENCES

- [1] S. S. Gershtein, V. V. Kiselev, A. K. Likhoded, and A. V. Tkabladze, Physics of  $B_c$ -mesons, Phys. Usp. **38**, 1 (1995).
- [2] P. G. Ortega, J. Segovia, D. R. Entem, and F. Fernandez, Spectroscopy of  $\mathbf{B}_c$  mesons and the possibility of finding exotic  $\mathbf{B}_c$ -like structures, Eur. Phys. J. C **80**, 223 (2020), arXiv:2001.08093 [hep-ph].
- [3] S. Donati, Prospects for B physics at the tevatron and LHCb, J. Phys.: Conf. Ser. **53**, 234 (2006).
- [4] F. Abe *et al.* (CDF Collaboration), Observation of the  $B_c$  meson in  $p\bar{p}$  collisions at  $\sqrt{s} = 1.8$  tev, Phys. Rev. Lett. **81**, 2432 (1998).
- [5] A. M. Sirunyan *et al.* (CMS Collaboration), Observation of two excited  $B_c^+$  states and measurement of the  $B_c^+(2s)$  mass in  $pp$  collisions at  $\sqrt{s} = 13$  TeV, Phys. Rev. Lett. **122**, 132001 (2019).
- [6] R. L. Workman *et al.* (Particle Data Group), Review of Particle Physics, Prog. Theor. Exp. Phys. **2022**, 083C01 (2022), <https://academic.oup.com/ptep/article-pdf/2022/8/083C01/49175539/ptac097.pdf>.
- [7] S. Capstick and S. Godfrey, Pseudoscalar decay constants in the relativized quark model and measuring the CKM matrix elements, Phys. Rev. D **41**, 2856 (1990).
- [8] C.-H. Chang and Y.-Q. Chen, Decays of the  $B_c$  meson, Phys. Rev. D **49**, 3399 (1994).
- [9] A. A. El-Hady, M. A. K. Lodhi, and J. P. Vary,  $B_c$  mesons in a Bethe-Salpeter model, Phys. Rev. D **59**, 094001 (1999).
- [10] M.-T. Choi and J. K. Kim, Determination of  $|V_{cb}|$  from the polarization of vector meson in the semileptonic decay of  $B$  and  $B_c$  meson, Phys. Lett. B **419**, 377 (1998).
- [11] E. J. Eichten and C. Quigg, Mesons with beauty and charm: Spectroscopy, Phys. Rev. D **49**, 5845 (1994).
- [12] S. S. Gershtein, V. V. Kiselev, A. K. Likhoded, and A. V. Tkabladze,  $B_c$  spectroscopy, Phys. Rev. D **51**, 3613 (1995).
- [13] J. Zeng, J. W. Van Orden, and W. Roberts, Heavy mesons in a relativistic model, Phys. Rev. D **52**, 5229 (1995).
- [14] I. F. Allison, C. T. H. Davies, A. Gray, A. S. Kronfeld, P. B. Mackenzie, and J. N. Simone (HPQCD, Fermilab Lattice, and UKQCD Collaborations), Mass of the  $B_c$  meson in three-flavor lattice qcd, Phys. Rev. Lett. **94**, 172001 (2005).
- [15] E. Gebrehana, S. Bhatnagar, and H. Negash, Analytic approach to calculations of mass spectra and decay constants of heavy-light quarkonia in the framework of bethe-salpeter equation, Phys. Rev. D **100**, 054034 (2019).
- [16] D. Ebert, R. N. Faustov, and V. O. Galkin, Spectroscopy and Regge trajectories of heavy quarkonia and  $B_c$  mesons, Eur. Phys. J. C **71**, 1825 (2011), arXiv:1111.0454 [hep-ph].
- [17] E. Eichten, K. Gottfried, T. Kinoshita, J. Kogut, K. D. Lane, and T. M. Yan, Spectrum of charmed quark-antiquark bound

- states, Phys. Rev. Lett. **34**, 369 (1975).
- [18] E. Eichten, K. Gottfried, T. Kinoshita, K. D. Lane, and T. M. Yan, Charmonium: The model, Phys. Rev. D **17**, 3090 (1978).
- [19] S. Godfrey, Spectroscopy of  $B_c$  mesons in the relativized quark model, Phys. Rev. D **70**, 054017 (2004).
- [20] O. Lakhina and E. S. Swanson, Dynamic properties of charmonium, Phys. Rev. D **74**, 014012 (2006).
- [21] S. N. Gupta, S. F. Radford, and W. W. Repko, Quarkonium spectra and quantum chromodynamics, Phys. Rev. D **26**, 3305 (1982).
- [22] S. F. Radford and W. W. Repko, Potential model calculations and predictions for heavy quarkonium, Phys. Rev. D **75**, 074031 (2007).
- [23] B.-Q. Li and K.-T. Chao, Higher charmonia and X, Y, Z states with screened potential, Phys. Rev. D **79**, 094004 (2009).
- [24] T. Barnes, S. Godfrey, and E. S. Swanson, Higher charmonia, Phys. Rev. D **72**, 054026 (2005).
- [25] R. Chaturvedi and A. Kumar Rai, Mass spectra and decay properties of the  $c\bar{c}$  meson, Eur. Phys. J. Plus **133**, 220 (2018).
- [26] R. Manzoor, J. Ahmed, and A. Raya, A new variational approach and its application to heavy quarkonia, Rev. Mex. Fis. **67**, 33 (2021).
- [27] A. Bhaghyesh, Charmonium Properties Using the Discrete Variable Representation (DVR) Method, Adv. High Energy Phys. **2021**, 9991152 (2021), arXiv:2103.06445 [hep-ph].
- [28] F. Brau and C. Semay, The three-dimensional fourier grid hamiltonian method, J. Comput. Phys. **139**, 127 (1998).
- [29] H. Mutuk, Spin Averaged Mass Spectrum of Heavy Quarkonium via Asymptotic Iteration Method, Can. J. Phys. **97**, 1342 (2019), arXiv:1806.04440 [hep-ph].
- [30] A. K. Rai and P. C. Vinodkumar, Properties of  $B_c$  meson, Pramana - J. Phys. **66**, 953 (2006), arXiv:hep-ph/0606194.
- [31] H. Mutuk, Cornell Potential: A Neural Network Approach, Adv. High Energy Phys. **2019**, 3105373 (2019).
- [32] M. Pillai, J. Goglio, and T. G. Walker, Matrix numerov method for solving schrödinger's equation, Am. J. Phys. **80**, 1017 (2012).
- [33] Y. Sumino, 'Coulomb + linear' form of the static QCD potential in operator product expansion, Phys. Lett. B **595**, 387 (2004).
- [34] Y. Sumino, QCD potential as a "Coulomb-plus-linear" potential, Phys. Lett. B **571**, 173 (2003).
- [35] O. Andreev and V. I. Zakharov, Heavy-quark potentials and AdS/QCD, Phys. Rev. D **74**, 025023 (2006).
- [36] C. White, The cornell potential from general geometries in AdS/QCD, Phys. Lett. B **652**, 79 (2007).
- [37] Y. Kinar, E. Schreiber, and J. Sonnenschein,  $Q\bar{Q}$  potential from strings in curved space-time: classical results, Nucl. Phys. B **566**, 103 (2000), arXiv:hep-th/9811192.
- [38] G. S. Bali, QCD forces and heavy quark bound states, Phys. Rep. **343**, 1 (2001).
- [39] T. Kawanai and S. Sasaki, Charmonium potential from full lattice QCD, Phys. Rev. D **85**, 091503 (2012).
- [40] Y. Koma and M. Koma, Scaling study of the relativistic corrections to the static potential, PoS **LAT2009**, 122 (2009), arXiv:0911.3204 [hep-lat].
- [41] Y. Koma, M. Koma, and H. Wittig, Relativistic corrections to the static potential at  $O(1/m)$  and  $O(1/m^2)$ , PoS **LAT2007**, 111 (2007), arXiv:0711.2322 [hep-lat].
- [42] T. Kawanai and S. Sasaki, Potential description of the charmonium from lattice QCD, AIP Conf. Proc. **1701**, 050022 (2016), arXiv:1503.05752 [hep-lat].
- [43] A. Laschka, N. Kaiser, and W. Weise, Quark-antiquark potential to order  $1/m$  and heavy quark masses, Phys. Rev. D **83**, 094002 (2011).
- [44] A. Laschka, N. Kaiser, and W. Weise, Charmonium potentials: Matching perturbative and lattice QCD, Phys. Lett. B **715**, 190 (2012).
- [45] G. Pérez-Nadal and J. Soto, Effective-string-theory constraints on the long-distance behavior of the subleading potentials, Phys. Rev. D **79**, 114002 (2009).
- [46] D. Ebert, R. N. Faustov, and V. O. Galkin, Properties of heavy quarkonia and  $B_c$  mesons in the relativistic quark model, Phys. Rev. D **67**, 014027 (2003).
- [47] A. M. Badalian and D. S. Kuzmenko, Freezing of QCD coupling affects the short distance static potential, Phys. Rev. D **65**, 016004 (2001).
- [48] A. M. Badalian, Y. A. Simonov, and B. L. G. Bakker, Masses and decay constants of  $B_q$  mesons in the qcd string approach, in *High Energy Physics*, edited by A. Sissakian, G. Kozlov, and E. Kolganova, pp. 1091–1094, arXiv:hep-ph/0610193.
- [49] J.-B. Liu and M.-Z. Yang, Spectrum of the charmed and b-flavored mesons in the relativistic potential model, J. High Energ. Phys. **07**, 106, arXiv:1307.4636 [hep-ph].
- [50] N. Mathur, M. Padmanath, and S. Mondal, Precise predictions of charmed-bottom hadrons from lattice QCD, Phys. Rev. Lett. **121**, 202002 (2018).
- [51] L. M. Abreu, F. M. d. C. Júnior, and A. G. Favero, Bottom-charmed meson spectrum from a QCD approach based on the Tamm-Dancoff approximation, Phys. Rev. D **102**, 034002 (2020).
- [52] Q. Li, M.-S. Liu, L.-S. Lu, Q.-F. Lü, L.-C. Gui, and X.-H. Zhong, Excited bottom-charmed mesons in a nonrelativistic quark model, Phys. Rev. D **99**, 096020 (2019).
- [53] N. R. Soni, B. R. Joshi, R. P. Shah, H. R. Chauhan, and J. N. Pandya,  $Q\bar{Q}$  ( $Q \in \{b, c\}$ ) spectroscopy using the Cornell potential, Eur. Phys. J. C **78**, 592 (2018), arXiv:1707.07144 [hep-ph].
- [54] X.-J. Li, Y.-S. Li, F.-L. Wang, and X. Liu, Spectroscopic survey of higher-lying states of  $B_c$  meson family, Eur. Phys. J. C **83**, 10.1140/epjc/s10052-023-12237-9 (2023).
- [55] N. Akbar, F. Akram, B. Masud, and M. Atif Sultan, Conventional and hybrid  $B_c$  mesons in an extended potential model, Eur. Phys. J. A **55**, 10.1140/epja/i2019-12735-1 (2019).

- [56] R. Royen and V. F. Weisskopf, Hardon decay processes and the quark model, *Nuovo Cimento A* **50**, 617 (1967).
- [57] R. Barbieri, R. Gatto, R. Kögerler, and Z. Kunszt, Meson hyperfine splittings and leptonic decays, *Phys. Lett. B* **57**, 455 (1975).
- [58] W. Celmaster, Lepton-width suppression of vector-meson decays, *Phys. Rev. D* **19**, 1517 (1979).
- [59] N. Akbar, Decay Properties of Conventional and Hybrid  $B_c$  Mesons, *Phys. Atom. Nucl.* **83**, 899 (2020).
- [60] C. Sun, R.-H. Ni, and M. Chen, Decay constants of  $B_c(nS)$  and  $B_c^*(nS)$ , *Chin. Phys. C* **47**, 023101 (2023), arXiv:2209.06724 [hep-ph].
- [61] S. Tang, Y. Li, P. Maris, and J. P. Vary,  $B_c$  mesons and their properties on the light front, *Phys. Rev. D* **98**, 114038 (2018).
- [62] M. J. Baker, J. Bordes, C. A. Dominguez, J. Penarrocha, and K. Schilcher,  $B$  Meson Decay Constants  $f_{B_c}$ ,  $f_{B_s}$  and  $f_B$  from QCD Sum Rules, *J. High Energ. Phys.* **07**, 032, arXiv:1310.0941 [hep-ph].
- [63] Z.-G. Wang, Analysis of the vector and axialvector  $B_c$  mesons with QCD sum rules, *Eur. Phys. J. A* **49**, 131 (2013), arXiv:1203.6252 [hep-ph].
- [64] V. V. Kiselev, Decays of the  $B_c$  meson <https://doi.org/10.48550/arxiv.hep-ph/0308214> (2003), arXiv:hep-ph/0308214.
- [65] A. Abd El-Hady, J. H. Muñoz, and J. P. Vary, Semileptonic and nonleptonic  $B_c$  decays, *Phys. Rev. D* **62**, 014019 (2000).
- [66] A. P. Monteiro, M. Bhat, and K. B. V. Kumar,  $c\bar{b}$  spectrum and decay properties with coupled channel effects, *Phys. Rev. D* **95**, 054016 (2017).
- [67] N. Devlani and A. Rai, Masses and electromagnetic transitions of the  $B_c$  mesons, *Eur. Phys. J. A* **50**, 154 (2014).
- [68] B. Martín-González, P. G. Ortega, D. R. Entem, F. Fernández, and J. Segovia, Toward the discovery of novel  $B_c$  states: Radiative and hadronic transitions, *Phys. Rev. D* **106**, 054009 (2022).
- [69] A. Abd El-Hady, J. R. Spence, and J. P. Vary, Radiative decays of  $B_c$  mesons in a Bethe-Salpeter model, *Phys. Rev. D* **71**, 034006 (2005).
- [70] M. A. Sultan, N. Akbar, B. Masud, and F. Akram, Higher hybrid charmonia in an extended potential model, *Phys. Rev. D* **90**, 054001 (2014).
- [71] E. Omugbe, E. Inyang, I. Njoku, C. Martínez-Flores, A. Jahanshir, I. Okon, E. Eyube, R. Horchani, and C. Onate, Approximate mass spectra and root mean square radii of quarkonia using cornell potential plus spin-spin interactions, *Nucl. Phys. A* **1034**, 122653 (2023).